Supporting Material

Unconventional mechanics of lipid membranes: a potential role for mechanotransduction of hair cell stereocilia

Jichul Kim

Department of Mechanical Engineering, Stanford University, Stanford, California, USA

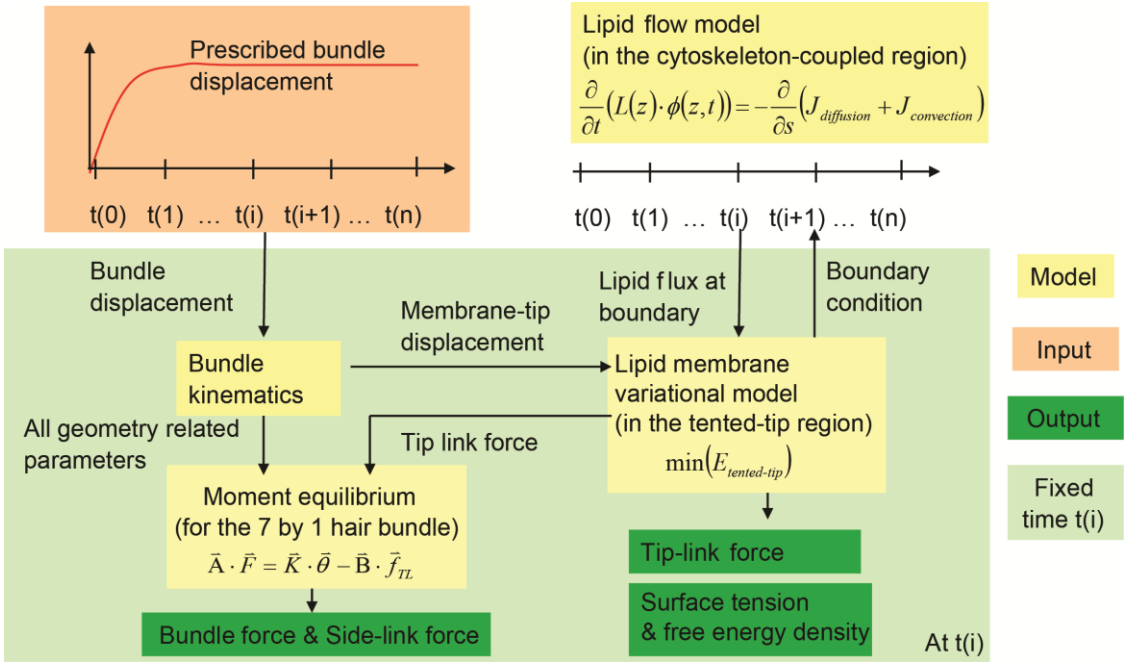

Figure S1. Multi-physics coupling. The presented multi-physics models are coupled and implemented by using *Matlab* (www.mathworks.com). Briefly, for a given input bundle displacement at time *t(i)*, motion of the seven stereocilia that comprise a bundle row is determined by using the kinematics of the system based on the sliding shear motion of the bundle. The membrane-tip displacement, calculated from the bundle kinematics, is taken as input for the lipid membrane deformation over the tented-tip region, which yields the tip-link force and membrane free energy density. In this variational model, surface tension of a constant state variable for the tented-tip region calculated from the previous state at time *t(i-1)* is used to predict the surface tension at *t(i)*. Finally, the tip-link force becomes the input for the system equation to calculate the bundle force and forces applied to the side links at *t(i)*. Hydrodynamics lipid transport in the cytoskeleton-coupled region, which is a time-dependent initial and boundary-value problem, is solved in parallel with the membrane variational model. These two models are coupled through the interface boundary condition. With this model, the temporal response of the tip-link force, hair-bundle force, and membrane free energy density at specific points in the tented-tip region with respect to hair bundle motion can be computed. See Materials and Methods section for descriptions of the equations

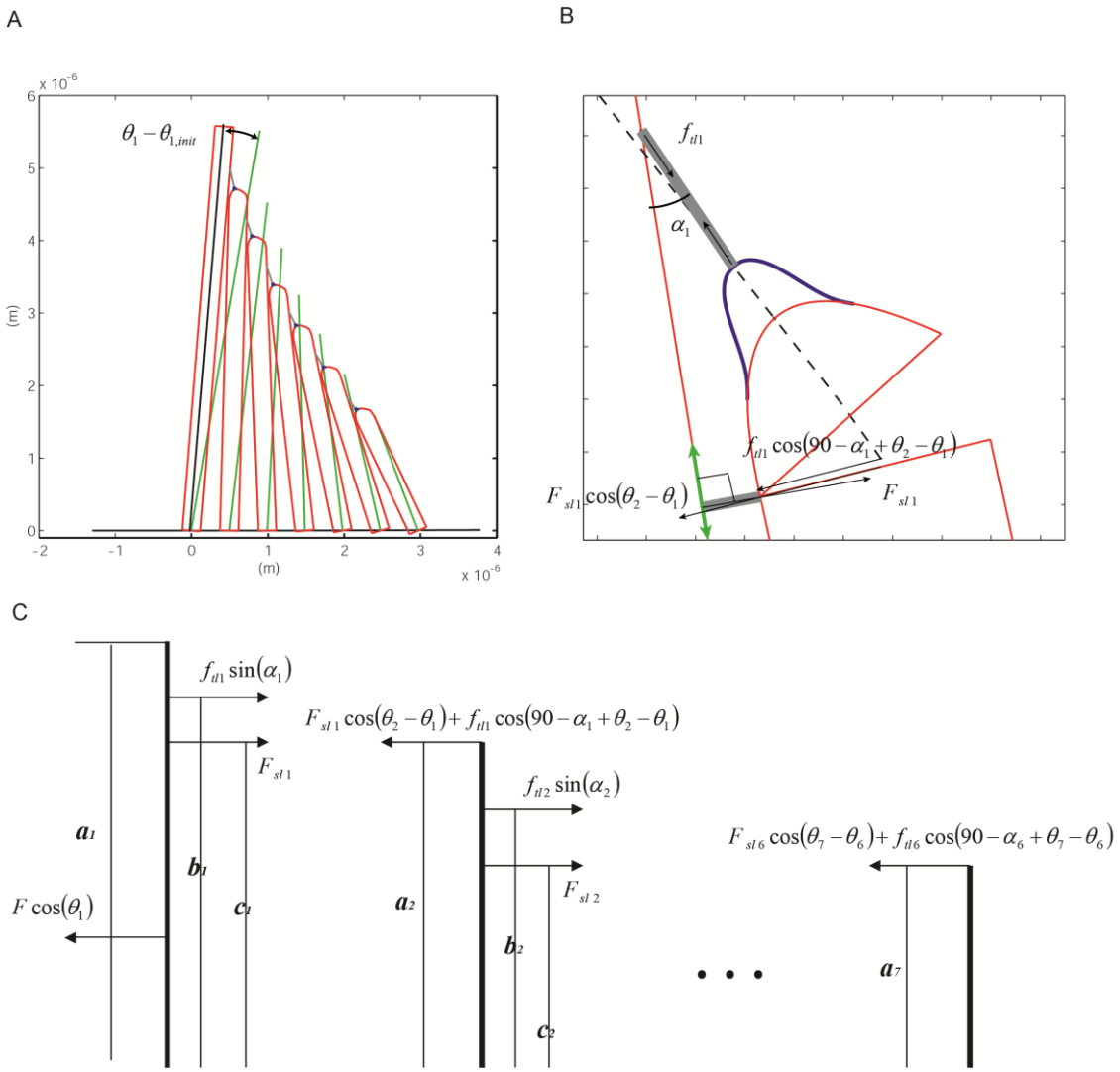

Figure S2. Kinematics component for the hair bundle model. (**A**) Hair bundle model configuration and dimensions. Green lines represent the initial resting central axis of each stereocilium. (**B**) Ciliary tip complex details and free body diagram. (**C**) Rotational free body diagram for the bundle's system equation. See Eq. 1 and Materials and Methods section for a description of the parameters.

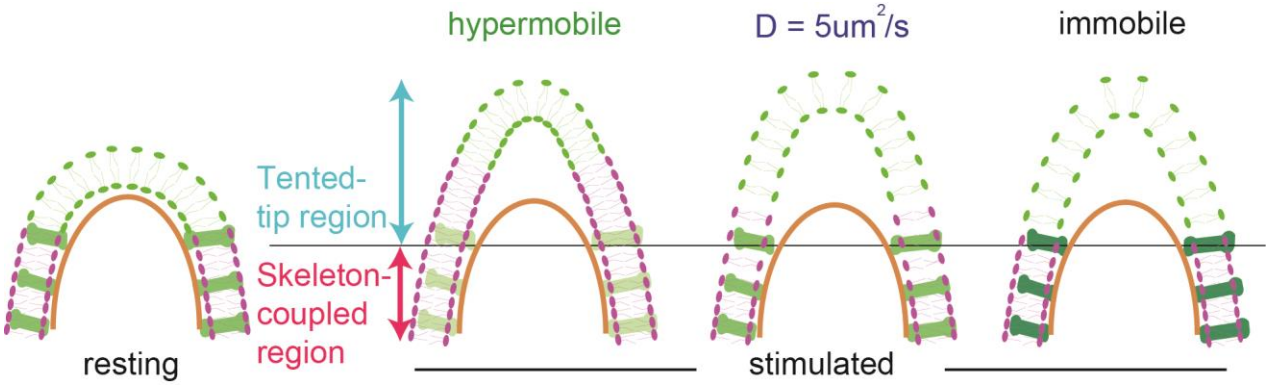

Figure S3. Illustration of the lipid flow in the stereocilia. Lipid flow in the cytoskeleton-coupled region (red arrow) is more viscous than that of the tented tip region (blue arrow) due to the frictional interaction between mobile lipids and anchored crosslinkers indicated with different intensity of green depending on the mobility of the systems. When the membrane is pulled under point stimuli, lipid densities in two regions are constant temporally and spatially for the hypermobile case. However, in the case of physiologically relevant lipid mobility (with D=5 $\mu m^2/s$), lower lipid density in the tented region and the density gradient in the cytoskeleton-coupled region are generated. Even though the case is physiologically and physically not relevant, the immobile case demonstrates the lowest lipid density in the tented region and an infinite gradient (i.e. discontinuity of the lipid density) at the interface. For all cases, the tented region is assumed to have a spatially uniform lipid density (i.e. quasi static). Two different colors for the lipid are used to trace the motion of the lipid with respect to the resting configuration. The thick brown line simply indicates the cytoskeleton i.e. actin core, and the thin black line indicates the interface between two regions of the lipid membrane.

Discussion for the parameters in the model

There are three types of parameters in this hair bundle model: parameters for the bundle, the ion channel, and the lipid membrane. First, the bundle parameters include the rotational stiffness of the rootlet and the geometric parameters demonstrated in Fig. S2. Since the rotational stiffness for the rootlet of the single stereocilium is unknown, this model parameter of 0.2 *fN/rad* is initially based on whole bundle measurements from rat outer hair cell bundles, where single stereocilia stiffness is calculated (1). This value is systematically adjusted to satisfy experimental force vs. displacement measurement from turtle with and without tip links. Second, the mechanosensitive ion channel parameters include area and internal energy difference between open and closed states of the channel. As mentioned in the main text, the internal energy difference of the hair cell MS channel is unknown, as the structural identity of the channel remains elusive. Therefore, a speculation on this free parameter of $7k_bT$ is based on the energy of a typical MS ion channel (2). For estimating the area difference of the channel of 3 nm^2, the size difference of the channel pore between an open and close state measured from a turtle is used (3). Third, lipid bilayer material properties for the tiny tip part of the stereocilia has not been directly tested thus far, and therefore selection of those values for this predictive research is based on previous research for the vesicle system or other cell types. The bending modulus for the lipid bilayer is in a range of 10-60k_bT (4-7) and it is closely correlated with the area stretching modulus, which is in a range of 110-650 *mN/m* (4, 5, 7). The nanoscopic diffusion constant for the tiny tip of the stereocilia also remains unknown. The confocal microscope measurement with 500 *nm* resolution estimates a microscopic diffusion constant of 1.1 $\mu m^2/s$ for the stereocilia (8). However, considering the tendency of underestimating the diffusion constant with low resolution experimental techniques (9), the nanoscopic diffusion constant for the stereocilia tip is expected to be greater than the measurement in (8). Finally, the resting lipid areal density ϕ_0 is taken from (10).

Detailed formulation for Eq. 10: Convective flux of lipids in the cytoskeleton-coupled region

In the cytoskeleton-coupled region, the convective flux of the lipid with drift velocity υ to the tangential direction of the membrane surface can be first written as follows

$$J_{convection}(s,t) = L(s)\cdot\phi(s,t)\cdot\upsilon(s,t) \quad \text{[S1]}$$

where s, L, and ϕ are the coordinate of the curve, the circumferential length of the stereocilia, and the lipid area density respectively. As depicted previously in the main text and in Fig.S4B, the drift velocity of the lipid here is driven by inter-molecular potential interaction and may be able to be parameterized by using the surface tension of the membrane. To formulate convective flux of lipids in detail, three concepts can be taken in order. First, the center of mass at which force f_c for driving drift of lipids is applied must be specified. For this purpose, one simple but reasonable approach is to define the mass as a pair of lipids at upper and lower leaflets for which the center of mass is located in the neutral plane of the membrane (see Fig. S4B). The second step is to formulate the applied force f_c at the center of mass in terms of gradient of the surface tension. This formulation is faithfully depicted below but again non-uniform stretching of the membrane due to the membrane-skeleton interaction is the basis of this surface tension gradient. Finally, this applied force f_c satisfies the equilibrium condition with the viscous drag force in the form of $f_{drag} = -\upsilon/\mu = -f_c$. Here, the coefficient μ is the mobility of the lipid membrane (i.e. inverse of the drag coefficient) (11, 12).

To formulate $f_c(s,t)$ it is necessary to consider a sectioned membrane area with infinitesimal arc length δs, as shown in Fig. S4A. At a fixed time, the net tensile force applied at $s=s_1$ in the tangential direction of the arc length is $\sigma(s_1)\cdot L(s_1)$. Similarly, it is $\sigma(s_2)\cdot L(s_2)$ at $s=s_2$. Since the number of lipids in the area from s_1 to s_2 i.e. $\int_{s1}^{s2}\phi(s)\cdot L(s)ds$ can be written as $\phi(s)\cdot L(s)\cdot\delta s$ when the infinitesimal arc length δs goes to zero, the tensile force applied for one center of mass at $s=s_1$ i.e. $f(s_1)$ can be calculated by normalizing the net force with respect to the number of center of mass in the sectioned area,

$$f(s_1) = \frac{2\sigma(s_1)\cdot L(s_1)}{\phi(s)\cdot L(s)\cdot\delta s} = \frac{2\sigma(s_1)}{\phi(s)\cdot\delta s} \quad \text{[S2]}$$

Here, in Eq. S2, "*2*" in the numerator represents two paired lipids at the upper and the lower leaflets for one center of mass. Similarly, the tensile force applied for one center of mass at $s=s_2$ is

$$f(s_2) = \frac{2\sigma(s_2)}{\phi(s)\cdot\delta s} \quad \text{[S3]}$$

From the general differential relationship for the quantity of σ along the arc length s as follows

$$\sigma(s_2) + \frac{\partial\sigma(s)}{\partial s}\cdot\delta s = \sigma(s_1) \quad \text{[S4]}$$

the applied force $f_c(s,t)$ can be expressed as follows in Eq. S5 by taking the difference of the tensile forces for the center of mass in the opposite direction (see Fig. S4 for the free body diagram).

$$f_c(s,t) = f(s_1,t) - f(s_2,t) = \frac{2\sigma(s_1)}{\phi(s)\cdot\delta s} - \frac{2\sigma(s_2)}{\phi(s)\cdot\delta s} = \frac{2}{\phi(s,t)}\frac{\partial\sigma(s,t)}{\partial s} \quad \text{[S5]}$$

The mobility of the lipid μ is parameterized with the diffusion constant by using the Einstein relation $\mu=D/(k_bT)$ (11-13). Finally, Eqns. S1 and S5 and the drift velocity of the form $\upsilon=-\mu f_{drag}=\mu f_c$ give the equation for the convective flux as follows

$$J_{convection}(z,t) = \frac{2D}{k_bT}L(z)\cdot\frac{\partial\sigma(z,t)}{\partial s} \quad \text{[S6]}$$

Here, k_b is Boltzmann's constant and T is temperature in Kelvin. The surface tension σ is a function of ϕ, which is given by Eq. 8.

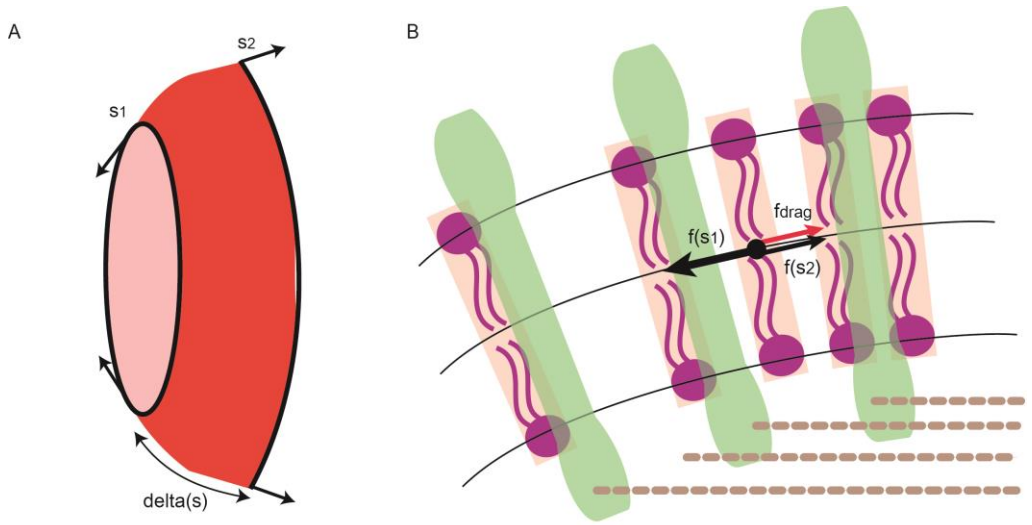

Figure S4. (**A**) Section of lipid membrane in the cytoskeleton-coupled region with infinitesimal arc length δs. Surface tensions at $s=s_1$ and $s=s_2$ are different when the membrane is non-uniformly stretched. (**B**) Paired lipids at the upper and the lower leaflets for which their center of mass (black dot) flows by following the neutral plane of the membrane. Thick-black and thin-black arrows indicate higher and lower tension applied on the center of mass in the opposite direction, respectively. The red arrow indicates viscous drag force in the opposite direction of the drift velocity. The viscous drag force is assumed to be generated by the interaction between lipids and crosslinkers (green) anchored to the cytoskeleton (dashed brown) (14). The difference between the two tensile forces (black arrows) lies in the force equilibrium with the drag force (red arrow), (i.e. $f(s_1)-f(s_2)=f_c=-f_{drag}$, where f_c is given by Eq. S5)

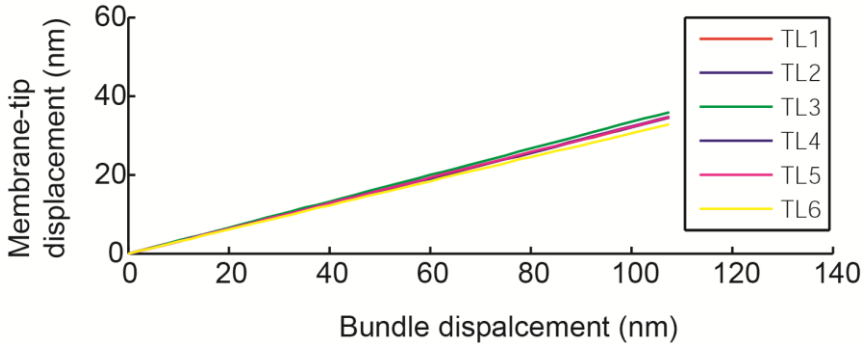

Figure S5. The membrane-tip displacement for each stereocilium in a row with respect to the bundle displacement. All six membrane-tip displacements are nearly consistent with the given stair-pattern bundle geometry. Sensitivity study of the bundle height indicates that as long as the staircase-pattern stereocilia geometry is reasonably defined, bundle kinematics yields negligible variation for the membrane-tip displacement for each stereocilium. This allows us to calculate only one membrane deformation that can be identically applied for all stereocilia. The result also supports the idea of simultaneous activation of the MS channels for the stereocilia with the bundle displacement.

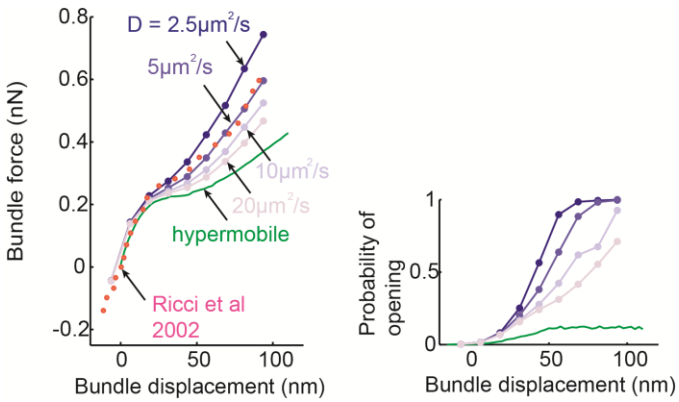

Figure S6. Sensitivity of the lipid mobility. (**Left**) Bundle force vs. displacement responses with respect to varying mobility of the lipid. The mobility of the lipid is parameterized by using diffusion constants through Einstein's relation. (**Right**) Probability of opening the channel that corresponds to the data in (Left). The membrane free energy density averaged from *r=3 nm* to *r=4.5 nm* are used. As demonstrated, the more lipids flow into the tented-tip region (with higher diffusion constants) the less probability of opening the channel is generated. The data suggest that the relaxational flow of lipids in the stereocilia might yield the automatic reclosure of the hair cell MS channel. See Table 1 for the parameters used.

Simulation data without consideration of the stiff protein region (Figs. S7 - S11 and Table 1S)

In the following section, simulation data without consideration of the stiff protein complex region are presented in figures from Fig. S7 to S11. Simulation settings and data formats are identical with that of the figures in the main text. Each of these from Fig. S7 to S11 corresponds to the main figures from Fig. 1 to Fig. 5 respectively.

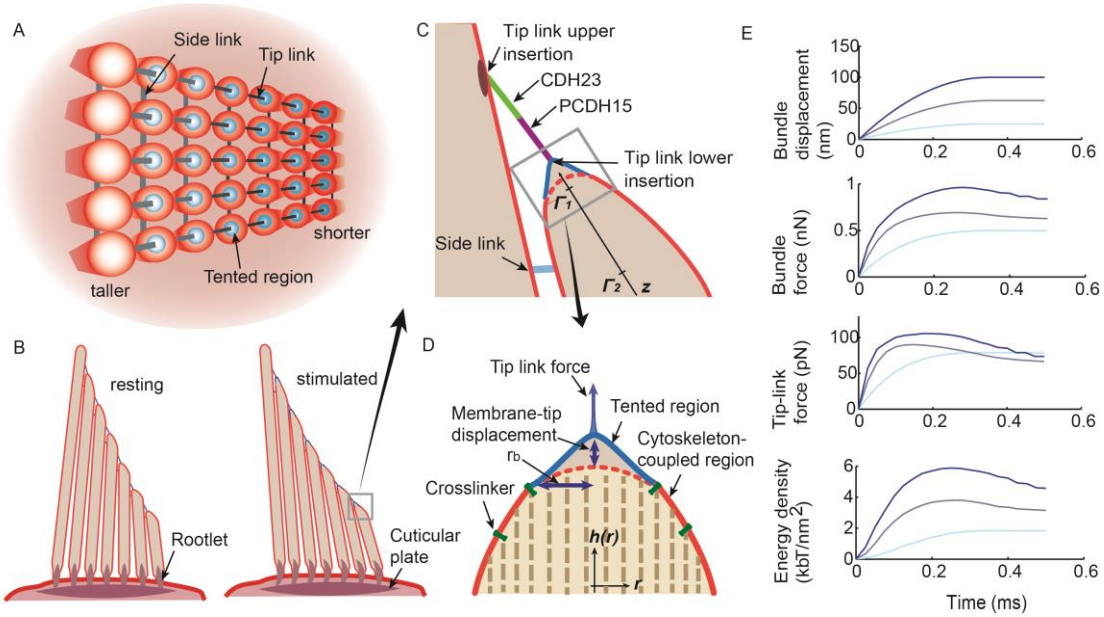

Figure S7. (***A***) Top view for stereocilia bundle. (***B***) Side view of the hair bundle. (***C***) Ciliary tip and tip link complex. (***D***) Partitioned lipid membrane for the stereocilia tip. The stiff region for membrane proteins presumably located in the tip region is not considered in this simulation. (***E***) Model responses to different size step functions (1st row). Bundle force (2nd row), single tip link force (3rd row), and membrane free energy density at a point 1nm from tip link lower insertion (4th row) are plotted. See Table S1 for the parameters used.

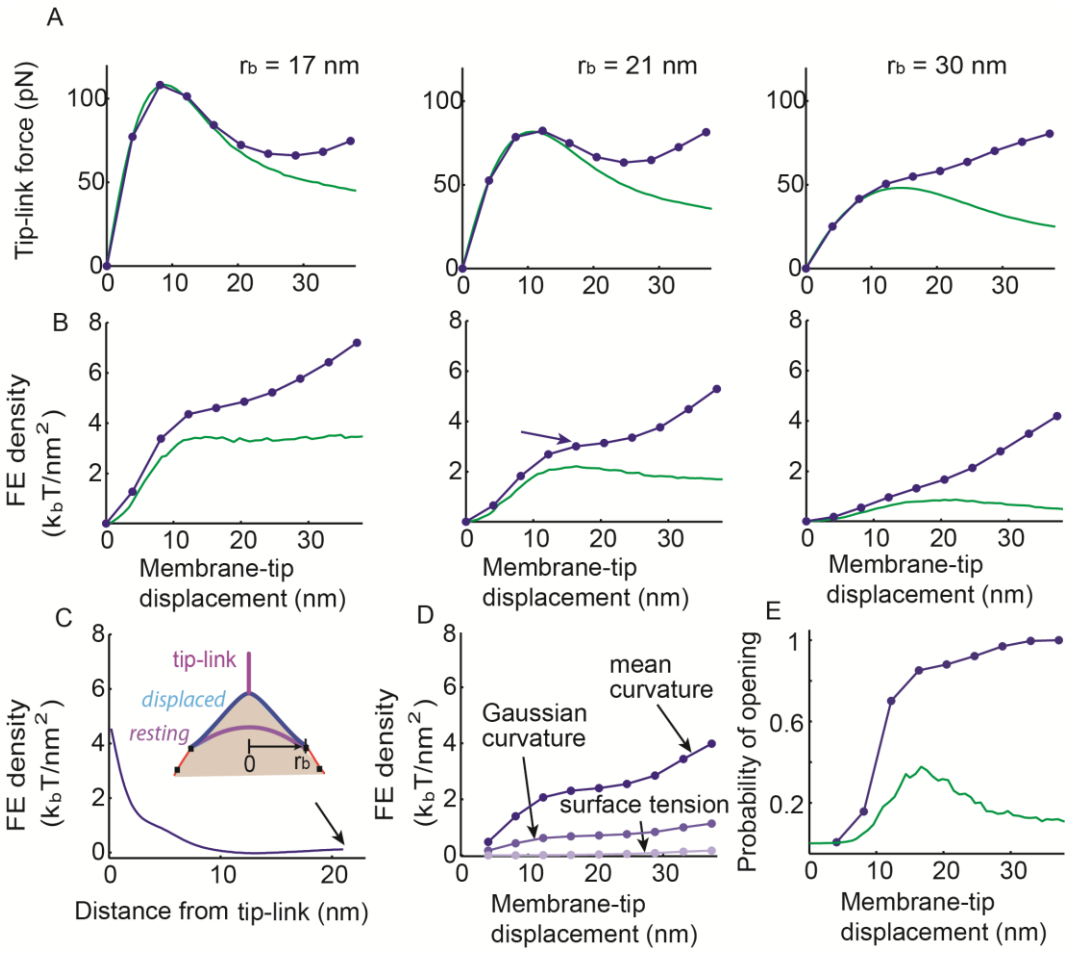

Figure S8. (***A***) Tip link force and (***B***) membrane free energy density at a point 1 nm from the tip link insertion site (i.e. *r* = 1 *nm*) with respect to membrane-tip displacement. Both responses are obtained at time=0.5 *ms* from the step stimuli stimulation shown in Fig. S1E. Data are indicated with linearly interpolated dots for $D=7\ \mu m^2/s$ case (blue). Hypermobility (green) of the lipid in the cytoskeleton-coupled region is also considered. 1st, 2nd, and 3rd columns of (*A*) and (*B*) use r_b=*17 nm, 21 nm*, and *30 nm*, respectively. (***C***) Free energy density profile of the tented-tip membrane corresponding to the arrowed data in (*B*), middle panel (r_b=*21 nm*). (***D***) Decomposed membrane free energy density shown with a blue trace in (*B*), middle panel. (***E***) Open probability of the MS channel using free energy density averaged from *r=0 nm* to *r=2 nm*. Both $D=7\ \mu m^2/s$ (blue) and hypermobility (green) cases are plotted. See Table S1 for the parameters used.

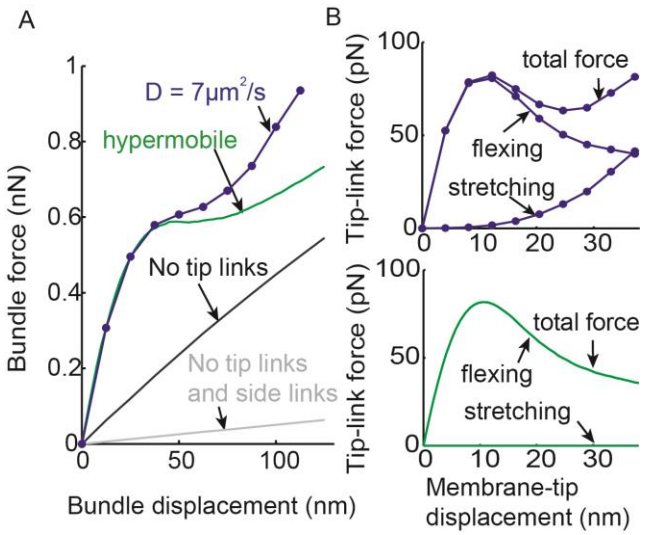

Figure S9. (***A***) From the tip-link force vs. membrane-tip displacement response in the middle panel of Fig. S8A (r_b=*21nm*), bundle force vs. displacement responses are plotted. Two different mobilities of the lipid in the cytoskeleton-coupled region are considered. Detachment of the tip links from the membrane linearized the response (black), and disconnecting side links as well further reduce the magnitude of the linear response (gray). (***B***) Membrane flexing and stretching components of the tip-link force. For each case of lipid mobility, the total single tip-link force is decomposed into two different force contributions. See Table S1 for the parameters used.

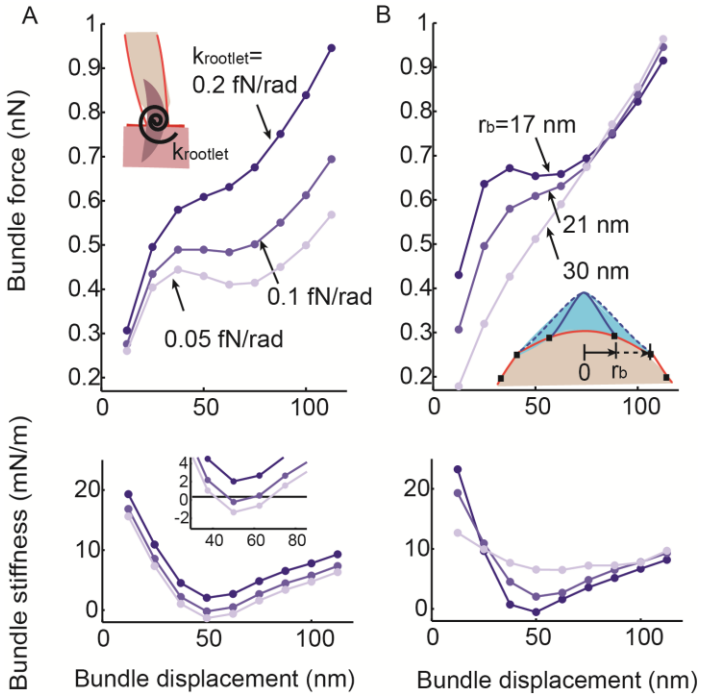

Figure S10. Using bundle force vs. displacement response with *D*=7 *μm²/s* in Fig. S9A, force (top) and stiffness (bottom), responses are calculated by varying the rotational stiffness of the rootlet in (***A***) with fixed r_b=21*nm*, and the parameter r_b in (**B**) with fixed $k_{rootlet}$=0.2*fN/rad*. See Table S1 for the parameters used.

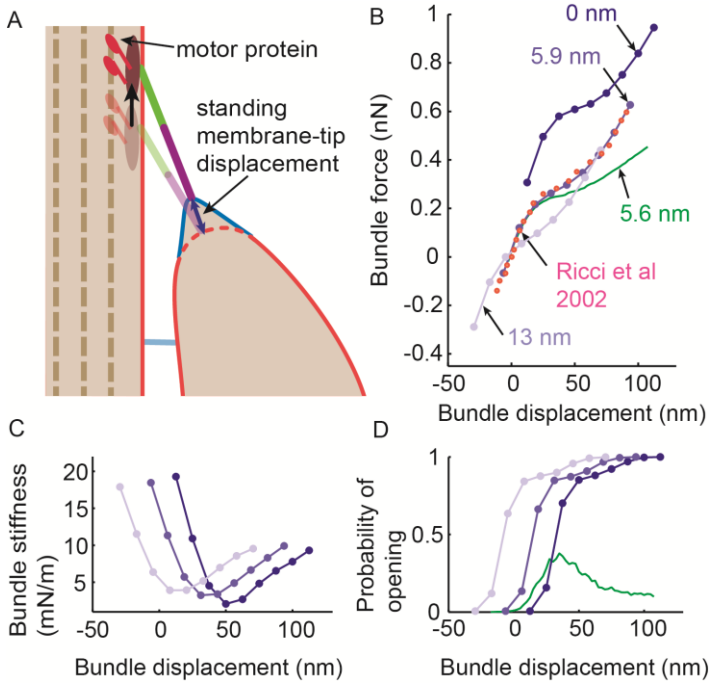

Figure S11. (***A***) Schematic representing a possible mechanism of applying a standing force to the tip link. (***B***) Hair bundle force vs. displacement plots with varying levels of the standing membrane-tip displacement (blue affiliation), using $D=7\ \mu m^2/s$ from Fig. S9A. The calculation correlating best with experimental data (magenta, Ricci et al. 2002) uses a standing membrane-tip displacement of 5.9 nm. (**C**) Bundle stiffness calculated from (B). (***D***) Open probability of the MS channel calculated using the membrane free energy density averaged from *r=0 nm* to *r=2 nm*. The hypermobile case (green) is also shown for (B) and (D). See Table S1 for the parameters used.

Table S1 Summary of the parameters used in Figs. S7 – S11 (***A***) The value is varied from 0.2 to 0.05 fN/rad in Fig. S10A. (***B***) This value is varied from 17 to 30 nm in Figs. S8AB and S10B.

Material properties	**Selected values**
Φ_0 (resting lipid areal density)	1000/629 x10^{18} /m^2
σ_0 (lipid bilayer surface tension with zero density strain)	exp(-7) *mN/m*
k_m (lipid bilayer bending modulus)	36k_bT
K_{app} (lipid bilayer apparent area stretching modulus)	300 *mN/m*
$k_{rootlet}$ (rootlet rotational stiffness of single stereocilium)	0.2 fN/rad [(A)]
D (lipid diffusion constant)	7 $\mu m^2/s$
$\Delta A_{channel}$ (hair cell MS channel area difference between open and closed states)	*3* nm^2
ΔG (hair cell MS channel internal energy difference between open and closed states)	7 k_bT
r_b (radial size of axisymmetric membrane)	21*nm* [(B)]

Supporting References

1. Beurg, M., J.-H. Nam, A. Crawford, and R. Fettiplace. 2008. The actions of calcium on hair bundle mechanics in mammalian cochlear hair cells. Biophysical journal 94:2639-2653.
2. Ursell, T., J. Kondev, D. Reeves, P. A. Wiggins, and R. RobPhillips. 2008. Role of lipid bilayer mechanics in mechanosensation. In Mechanosensitive Ion Channels. Springer. 37-70.
3. Farris, H., C. LeBlanc, J. Goswami, and A. Ricci. 2004. Probing the pore of the auditory hair cell mechanotransducer channel in turtle. The Journal of physiology 558:769-792.
4. Evans, E., and W. Rawicz. 1990. Entropy-driven tension and bending elasticity in condensed-fluid membranes. Physical Review Letters 64:2094.
5. Rawicz, W., K. Olbrich, T. McIntosh, D. Needham, and E. Evans. 2000. Effect of chain length and unsaturation on elasticity of lipid bilayers. Biophysical journal 79:328-339.
6. Powers, R. J., S. Roy, E. Atilgan, W. E. Brownell, S. X. Sun, P. G. Gillespie, and A. A. Spector. 2012. Stereocilia membrane deformation: Implications for the gating spring and mechanotransduction channel. Biophysical journal 102:201-210.
7. Solmaz, M. E., S. Sankhagowit, R. Biswas, C. A. Mejia, M. L. Povinelli, and N. Malmstadt. 2013. Optical stretching as a tool to investigate the mechanical properties of lipid bilayers. RSC advances 3:16632-16638.
8. de Monvel, J. B., W. Brownell, and M. Ulfendahl. 2006. Lateral diffusion anisotropy and membrane lipid/skeleton interaction in outer hair cells. Biophysical journal 91:364-381.
9. Marguet, D., P.-F. Lenne, H. Rigneault, and H.-T. He. 2006. Dynamics in the plasma membrane: how to combine fluidity and order. The EMBO journal 25:3446-3457.
10. Petrache, H. I., S. W. Dodd, and M. F. Brown. 2000. Area per Lipid and Acyl Length Distributions in Fluid Phosphatidylcholines Determined by< sup> 2</sup> H NMR Spectroscopy. Biophysical journal 79:3172-3192.
11. Hughes, B., B. Pailthorpe, and L. White. 1981. Translational and Rotational Drag on a Cylinder Moving in a Membrane. Journal of Fluid Mechanics 110:349-372.
12. Hochmuth, R. 1982. Solid and liquid behavior of red cell membrane. Annual review of biophysics and bioengineering 11:43-55.
13. Tirrell, M., and M. F. Malone. 1977. Stress-induced diffusion of macromolecules. Journal of Polymer Science: Polymer Physics Edition 15:1569-1583.
14. Kusumi, A., C. Nakada, K. Ritchie, K. Murase, K. Suzuki, H. Murakoshi, R. S. Kasai, J. Kondo, and T. Fujiwara. 2005. Paradigm shift of the plasma membrane concept from the two-dimensional continuum fluid to the partitioned fluid: high-speed single-molecule tracking of membrane molecules. Annu. Rev. Biophys. Biomol. Struct. 34:351-378.